

# Determining Microscopic Viscoelasticity in Flexible and Semiflexible Polymer Networks from Thermal Fluctuations

B. Schnurr, F. Gittes, F.C. MacKintosh, and C.F. Schmidt

Department of Physics & Biophysics Research Division,  
University of Michigan, Ann Arbor, MI 48109-1120

July 28, 1997

## Abstract

We have developed a new technique to measure viscoelasticity in soft materials such as polymer solutions, by monitoring thermal fluctuations of embedded probe particles using laser interferometry in a microscope. Interferometry allows us to obtain power spectra of fluctuating beads from 0.1 Hz to 20 kHz, and with subnanometer spatial resolution. Using linear response theory, we determined the frequency-dependent loss and storage shear moduli up to frequencies on the order of a kHz. Our technique measures local values of the viscoelastic response, without actively straining the system, and is especially suited to soft biopolymer networks. We studied semiflexible F-actin solutions and, as a control, flexible polyacrylamide (PAAm) gels, the latter close to their gelation threshold. With small particles, we could probe the transition from macroscopic viscoelasticity to more complex microscopic dynamics. In the macroscopic limit we find shear moduli at 0.1 Hz of  $G' = 0.11 \pm 0.03$  Pa and  $0.17 \pm 0.07$  Pa for 1 and 2 mg/ml actin solutions, close to the onset of the elastic plateau, and scaling behavior consistent with  $G^*(\omega) \sim \omega^{3/4}$  at higher frequencies. For polyacrylamide we measured plateau moduli of 2.0, 24, 100 and 280 Pa for crosslinked gels of 2, 2.5, 3 and 5% concentration (weight/volume) respectively, in agreement to within a factor of two with values obtained from conventional rheology. We also found evidence for scaling of  $G^*(\omega) \sim \omega^{1/2}$ , consistent with the predictions of the Rouse model for flexible polymers.

## Introduction

The usefulness of synthetic polymeric materials, and the functions of biopolymers, are all largely based on complex mechanical properties that derive from a hierarchi-

cal structure. The mechanical response of polymer solutions or gels displays characteristics of both fluids (viscosity) and of solids (elasticity), depending on the rate of change of applied stress. This response is conventionally described by frequency-dependent storage and loss shear moduli which are commonly measured by active, mechanically-imposed oscillatory strain in macroscopic samples, in contrast to stationary-flow geometries used for measurements in fluids<sup>1–5</sup>.

Such methods have also been used in the past to study reconstituted biopolymer networks *in vitro*. A general distinction between synthetic polymers and biopolymers is that the former are typically flexible, since their monomer size is small, whereas many biopolymers are formed from large protein monomers and thus are much less flexible. The viscoelastic properties of flexible and semiflexible polymer systems are quite different. At a given volume fraction of polymer, the shear modulus (or stiffness) of a semiflexible polymer network can be several orders of magnitude larger than that of a flexible one. This may be one reason why biological evolution has favored semiflexible polymer networks for mechanical stability. F-actin is one of the primary components of the *cytoskeleton* of plant and animal cells, and is largely responsible for the viscoelastic response of cells<sup>6,7</sup>. The  $\sim 17 \mu\text{m}$  persistence length of actin filaments<sup>8,9</sup> is about three orders of magnitude larger than their diameter. This tremendous aspect ratio makes them ideal model semiflexible polymers. They are rather rigid on the scale of cytoskeletal networks of typical cells, which have characteristic mesh sizes on the order of microns. In reconstituted F-actin networks, individual filaments can be hundreds of microns long, so that solutions of less than 0.1% polymer (volume fraction) are still strongly entangled.

Macroscopic rheological measurements in reconstituted F-actin solutions have been reported in the

literature<sup>10–19</sup>. These experiments have shown that the regime of linear viscoelastic response is small,<sup>16</sup> of order a few percent, and that this range decreases with increasing F-actin concentration. For larger strains, strain hardening is observed, followed by apparent shear thinning, which may be due to filament breakage. This is to be expected for semiflexible polymer networks, since the amplitudes of thermal undulations are small, and the full extension of individual filaments is thus reached for small strains,<sup>20</sup> making the response nonlinear. This makes measurements with commercial rheometers problematic, although some custom instruments can deal with strains substantially smaller than 1%.<sup>1</sup> Active macroscopic measurements on actin have given controversial results<sup>16</sup> and nonlinearity may be one reason for this.

In attempts to approach *in vivo* conditions, viscoelasticity has also been studied on a microscopic, cellular scale. Early work included the manipulation of magnetic particles in gelatin<sup>21</sup> and in living cells<sup>22</sup>. Recent experimental techniques for manipulating and tracking sub-micrometer particles have revived the interest in *microrheology*. Several studies have used direct manipulation of embedded magnetic beads in solutions of F-actin<sup>23–27</sup>. These experiments have been limited by the spatial and temporal resolution of video microscopy.

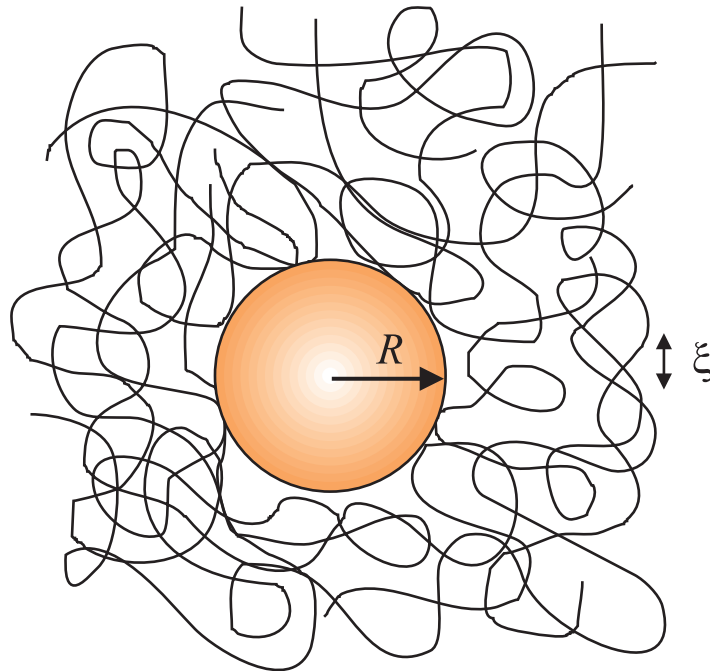


Figure 1: Schematic of a probe particle of radius  $R$  embedded in an actin network of mesh size  $\xi$ .

We introduce here a microscopic method of measuring viscoelastic properties within micrometer-sized sample volumes. We study entangled, but non-crosslinked networks of semiflexible F-actin, as well as low vol-

ume fraction gels of crosslinked polyacrylamide (PAAm), a flexible polymer. We observe the thermal fluctuations of micrometer-sized particles embedded in soft gels (Fig. 1). Laser interferometry in a light microscope provides high resolution (less than 1 nm) and bandwidth (from 0.1 Hz to 20 kHz). Using dispersion relations from linear response theory, the frequency-dependent loss and storage shear moduli can be determined from the fluctuation power spectra. The technique is in principle less invasive than active methods, in that no strain at all is imposed on the material.

Diffusing wave spectroscopy (DWS) has been used by others to observe thermal fluctuations of ensembles of particles, and viscoelastic properties in polymers and colloids have thereby been deduced<sup>28,29</sup>. This method measures average viscoelastic properties, as opposed to our local measurements; we further compare this conceptually related method with ours in the Discussion.

Our method measures shear moduli over a larger frequency range than accessible to video based microrheology (while DWS and some other macroscopic methods can reach higher frequencies<sup>1,30</sup>). Besides providing a new way of passively measuring shear moduli in both synthetic and biological polymer systems, our technique can be sensitive to dynamics and material parameters that are inaccessible to macroscopic methods: spatial inhomogeneities in networks can be studied on a micrometer scale. At low frequencies, our method appears to be sensitive to dynamics, such as non-shear deformations of the network with respect to the solvent, that are not seen in macroscopic mechanical rheology. For probe sizes comparable to the mesh size of the polymer network, deviations from continuum elasticity become apparent. With decreasing probe size, the transition from collective network dynamics to single-filament dynamics can be traced to explore the microscopic basis for macroscopic properties. This is particularly relevant for biopolymer networks, with mesh sizes as large as microns. More importantly for biology, microrheology will permit the characterization of small samples, such as living cells.

## Theory and Data Analysis Methods<sup>31</sup>

We model our experiments as embedding a spherical bead, of radius  $R$ , in a linear viscoelastic medium of density  $\rho$  with a macroscopic complex shear modulus  $G^*$  and Poisson ratio  $\nu$ .<sup>32</sup> For motions of micron-sized probe particles, inertial effects are negligible at frequencies  $\omega$  where the inertial decay length (i.e., the inverse magnitude  $1/|\Gamma|$  of the complex propagation constant<sup>1</sup>  $\Gamma = (\rho\omega^2/2G^*)^{1/2}$ ) is larger in magnitude than  $R$ . At

1 kHz,  $1/|\Gamma|$  is at least tens of microns in all our samples. Correspondingly, inertial effects can be expected to be relevant only for frequencies of order 1 MHz. In addition, the Reynolds number for thermal motions on this scale is small:  $\sim 10^{-3}$ . In an incompressible medium, bead motion is then determined entirely by the frequency-dependent complex shear modulus  $G^*(\omega) = G'(\omega) + iG''(\omega)$ , where  $G'$  and  $G''$  are the storage and loss moduli.

In extremely low-frequency motions of a gel, the network deforms so slowly that stress in the solvent relaxes completely, and the network can undergo not only shear but compressional deformation, i.e. it behaves as an elastic continuum with shear modulus  $G \equiv G^*(\omega = 0)$  and Poisson ratio  $\nu < 1/2$ . Stress  $\sigma_{ij}$  is related to strain  $u_{ij}$  by<sup>32</sup>

$$\sigma_{ij} = 2G [u_{ij} + \nu \delta_{ij} \Sigma u_{kk} / (1 - 2\nu)]. \quad (1)$$

The equation of elastic equilibrium,  $\partial\sigma_{ij}/\partial x_i = 0$ , can be solved exactly for  $u_{ij}$  with no-slip boundary conditions on a rigid spherical surface,<sup>33–35</sup> yielding an effective compliance (reciprocal spring constant) for sphere displacement

$$\alpha(\omega = 0) = \frac{1}{6\pi GR} \left[ 1 + \frac{(\nu - 1/2)}{2(\nu - 1)} \right]. \quad (2)$$

The static compliance  $\alpha$  in the limit  $\omega \rightarrow 0$  is significant because it is related by equipartition of energy to the total mean square fluctuations of the probe particle in the gel:

$$\langle x^2 \rangle = kT\alpha(\omega = 0). \quad (3)$$

Eqs. (3) and (2) together provide an estimate of the static modulus  $G$  from the variance  $\langle x^2 \rangle$  of fluctuations: a priori,  $\nu$  is unknown in Eq. (2) but over the relevant range,  $0 < \nu \leq 1/2$ ,  $\nu$  does not strongly affect the result; one can put  $\alpha \approx 1/6\pi GR$  with at most 25% error. However,  $\langle x^2 \rangle$  is often dominated by low-frequency instrumental drifts. We will instead use a method (to be described below) of estimating  $G^*(\omega = 0)$  that is less sensitive to such noise.

For frequencies above the  $\omega \rightarrow 0$  limit, viscous stresses develop in the gel, and we must reconsider Eq. (2). The solvent and the polymer network are coupled through viscous drag, which becomes stronger with increasing frequency. Eventually, solvent and network are expected to move as one at scales large compared with the network mesh size  $\xi$ . In this case the polymer network is strongly coupled to the incompressible solvent and so behaves like an incompressible network, which can be described by a Poisson ratio  $\nu = 1/2$ . The crossover frequency, above

which incompressible behavior is observed, can be estimated as follows. The viscous force per volume exerted by the solvent on the network<sup>36,37</sup> is  $\sim \eta v / \xi^2$ , where  $v$  is the velocity of the solvent relative to the network. The local elastic force per volume (exerted by the rest of the network) is  $G \nabla^2 u \sim u / R^2$  at the bead surface, where  $u$  is the network displacement field. Viscous coupling will dominate above a crossover frequency

$$\omega_c \simeq \frac{G}{\eta} \frac{\xi^2}{R^2}. \quad (4)$$

Eq. (4) is an order-of-magnitude estimate of  $\omega_c$  that corresponds to a few Hertz in our F-actin solutions ( $G \simeq 1$  Pa,  $\xi \simeq 0.1R$ ,  $\eta = 1$  cP). Above  $\omega_c$ , provided that  $\xi$  is small compared with  $R$ , the bead moves as an inclusion in an incompressible continuum viscoelastic medium. The stress-strain relations in Eq. (1) still hold, but with  $\nu = 1/2$ . The spatial equation of motion is still  $\partial\sigma_{ij}/\partial x_i = 0$  (at a given  $\omega$ ) and its solution is Eq. (2) with  $\nu = 1/2$ :

$$x_\omega = \alpha^*(\omega) f_\omega = \frac{1}{6\pi G^*(\omega) R} f_\omega. \quad (5)$$

$\alpha^*(\omega)$  and  $G^*(\omega)$  are complex because this formula describes sinusoidal sphere displacements  $x(t) = \alpha^*(\omega) f(t)$  caused by a force  $f(t) \propto e^{-i\omega t}$ . This is a generalization of the well-known Stokes formula  $f = 6\pi\eta r\dot{x}$ , since  $\eta = iG^*(\omega)/\omega$  in a purely viscous fluid.

We can rigorously justify Eq. (5) directly, as follows. It applies to an incompressible medium without inertia. The dynamics of the medium are completely determined by its stress-strain relation (Eq. (1)), which becomes  $\sigma_{ij} = 2G^*(\omega)u_{ij}$ . This is mathematically the same law that describes a simple viscous fluid, but with the (complex and frequency-dependent) quantity  $iG^*(\omega)/\omega$  replacing the viscosity  $\eta$ . Together with the equation of motion,  $\partial\sigma_{ij}/\partial x_i = 0$ , the spatial equations to be solved are also mathematically identical. The unique solution to these equations at a frequency  $\omega$ , that satisfies no-slip boundary conditions on the surface of the moving sphere, is precisely the Stokes law, with the (complex and frequency-dependent)  $G^*(\omega)$  replacing the quantity  $-i\omega\eta$ . This has the simple and remarkable consequence that the well-known Stokes force generalizes to give the correct compliance, involving the complex  $G^*(\omega)$ .

For  $\omega$  between zero and  $\omega_c$ , the solvent and network may undergo significant relative motion. As a result of this partial “draining” of the network, Eq. (5) will not be valid; the situation must then be described by a “two-fluid” model<sup>36,37</sup>. Force response and fluctuations may become dominated by long-wavelength modes that

relax over distances large compared with  $\xi(G/\eta\omega)^{1/2}$ . This low-frequency draining allows for relative motion of network and solvent, involving not only shear modes but also compressional modes in the network. As the spatial extent of the modes becomes larger than the bead size, the bead motion and its power spectrum are expected to become independent of bead size.

The compliance  $\alpha^*(\omega) = \alpha'(\omega) + i\alpha''(\omega)$  is the complex response function for bead displacement. Thus, for frequencies above  $\omega_c$ , Eq. (5) and the fluctuation-dissipation theorem<sup>38</sup> relate  $\langle x_\omega^2 \rangle$ , the power spectral density (PSD) of thermal motion, to the imaginary part  $\alpha''(\omega)$ :

$$\langle x_\omega^2 \rangle = \frac{4kT\alpha''(\omega)}{\omega}. \quad (6)$$

Provided that  $\alpha''(\omega)$  is known over a large enough frequency range, one can recover the real compliance  $\alpha'(\omega)$  from the Kramers-Kronig relations<sup>38</sup> by evaluating a dispersion integral

$$\alpha'(\omega) = \frac{2}{\pi} P \int_0^\infty d\zeta \frac{\zeta \alpha''(\zeta)}{\zeta^2 - \omega^2} \quad (7)$$

$$= \frac{2}{\pi} \int_0^\infty dt \cos \omega t \int_0^\infty d\zeta \alpha''(\zeta) \sin(\zeta t). \quad (8)$$

This allows us to explicitly calculate (by Eqs. (5) and (6)) the storage and loss moduli  $G'(\omega)$  and  $G''(\omega)$ .  $P$  in Eq. (7) denotes a principal-value integral, meaning the  $\epsilon \rightarrow 0$  limit of the sum of two  $\zeta$ -integrals: from 0 to  $(\omega - \epsilon)$ , and from  $(\omega + \epsilon)$  to  $\infty$ . However, as written in Eq. (8), this is equivalent to successive sine and cosine transforms of  $\alpha''(\omega)$ , which are conveniently performed for the discrete data points of a long time series. Standard Fourier routines<sup>39</sup> can be used to evaluate the discrete PSD and then to perform the sine and cosine transforms. Either the PSD or the output of Eq. (8) can be smoothed (by averaging within bins of equal logarithmic spacing) without strongly affecting the numerical results. As a control, we have also calculated Eq. (7) directly in the logarithmic domain, finding similar results.

When the behavior of the network plus solvent is well described as a single-component medium (so that Eq. (5) holds), we can take the complex reciprocal of  $\alpha^*(\omega)$  to obtain the complex  $G^*(\omega)$ :

$$G'(\omega) = \frac{1}{6\pi R} \frac{\alpha'(\omega)}{\alpha'(\omega)^2 + \alpha''(\omega)^2}, \quad (9)$$

$$G''(\omega) = \frac{1}{6\pi R} \frac{-\alpha''(\omega)}{\alpha'(\omega)^2 + \alpha''(\omega)^2}. \quad (10)$$

Qualitatively, we expect the shear modulus  $G^*(\omega)$  to exhibit a characteristic form,<sup>4</sup> involving up to three distinct dynamical regimes. If the polymer network is en-

tangled but not crosslinked, as in F-actin solutions, viscous flow will occur over times longer than the reptation time  $\tau_r$ , with  $G'(\omega)$  going to zero. The reptation time is hours or days, for actin filaments tens of microns long,<sup>40</sup> and is thus not accessible to our experiments. For frequencies above  $1/\tau_r$ , a rubber-like plateau appears, with a frequency-independent elastic response  $G'$ , as in a crosslinked gel. Above the high-frequency end of the plateau, the moduli are expected to increase with a characteristic power of frequency,  $G' \sim \omega^z$  and  $G'' \sim \omega^z$ , reflecting the increasingly limited relaxations of dynamic modes within a mesh of the network<sup>4</sup>. Power law behavior is expected for the shear moduli of any polymer network above the characteristic mesh relaxation time and below the molecular high frequency cut-off, since there is no other characteristic length or time scale in this regime. In this scaling regime, from Eqs. (5) and (6), the PSD is then expected to follow

$$\langle x_\omega^2 \rangle \sim \omega^{-(1+z)}. \quad (11)$$

## Materials and Experimental Methods

Actin was purified (~95% purity) from chicken skeletal muscle, following standard recipes<sup>41</sup>. Its concentration was determined both by staining (BioRad) and by UV absorption at 290 nm (specific absorption: 0.65 cm<sup>2</sup>/mg). Monomeric actin (G-actin) was rapidly frozen in liquid nitrogen and stored at -85°C. Samples were prepared by mixing G-actin with a small number of silica beads (Bangs Laboratories, except for the 0.5 μm diameter beads, which were kindly provided by E. Matijevic). After adding concentrated polymerization buffer (F-buffer: 2 mM hydroxyethyl-piperazineethanesulfonic acid (HEPES) (pH 7.2), 2 mM MgCl<sub>2</sub>, 50 mM KCl, 1 mM ethylenebis(oxyethylenenitrilo)tetraacetic acid (EGTA), 1 mM adenosinetriphosphate (ATP)) the mixture was immediately transferred into a sample chamber made from a microscope slide, a cover slip and double-stick tape (with inner dimensions 15mm×3mm×70μm). In the sealed sample chamber the actin polymerized at room temperature for at least one hour under slow rotation. The samples were stored at 4°C and examined within one day (and in one case remeasured the following day, as a control).

Polyacrylamide (PAAm) gels were prepared according to a standard gel electrophoresis recipe,<sup>42</sup> with concentrations of 2, 2.5, 3 and 5% (weight/volume) and a relative concentration of 3% bis-acrylamide as a crosslinker. Solutions were thoroughly degassed under vacuum, beads added and polymerization initiated with tetramethylmethylenediamine (TEMED) and ammonium persulfate (APS). As with actin, polymerizing

solutions were then transferred into sample chambers ( $15\text{mm} \times 6\text{mm} \times 140\mu\text{m}$ ) and slowly rotated at room temperature for at least one hour before starting experiments.

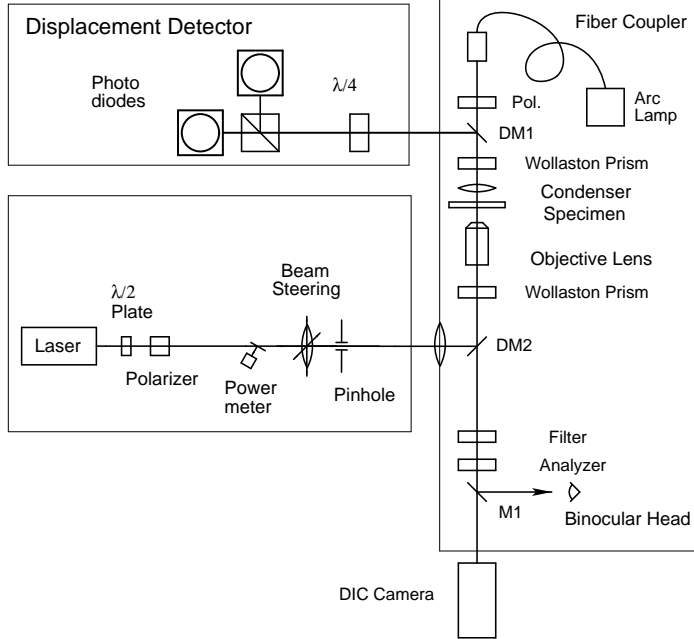


Figure 2: Schematic diagram of the custom-built inverted light microscope used for differential interference contrast imaging and laser interferometric displacement detection.

Our microscope is a custom-built inverted instrument (optics from Carl Zeiss, Inc.), constructed on an optical rail system and mounted on a vibration isolated optical bench (Fig. 2). To detect the thermal motion of beads imbedded in the gel we used an interferometer<sup>43,44</sup> (see Fig. 3) with near-infrared laser illumination (1064 nm NdVO<sub>4</sub>, 3.4 W (cw) max. power, Topaz 106c, Spectra Physics).

A linearly polarized laser beam is split in two beams by the Wollaston prism below the objective, which produces two diffraction limited overlapping foci in the specimen plane. A refractive particle located asymmetrically within the two foci will cause slightly elliptical polarization after recombination of the two beams by the upper Wollaston prism. A quarter-wave plate renders the light close to circularly polarized, whose two perpendicular linear components are then detected by two photodiodes. Deviations from circularity are calibrated to measure particle displacements. The normalized difference between the two signals is calculated by custom-built analog electronics (Fig. 3), amplified and anti-alias filtered slightly below the Nyquist frequency. This analog signal is then digitized and recorded using an A/D in-

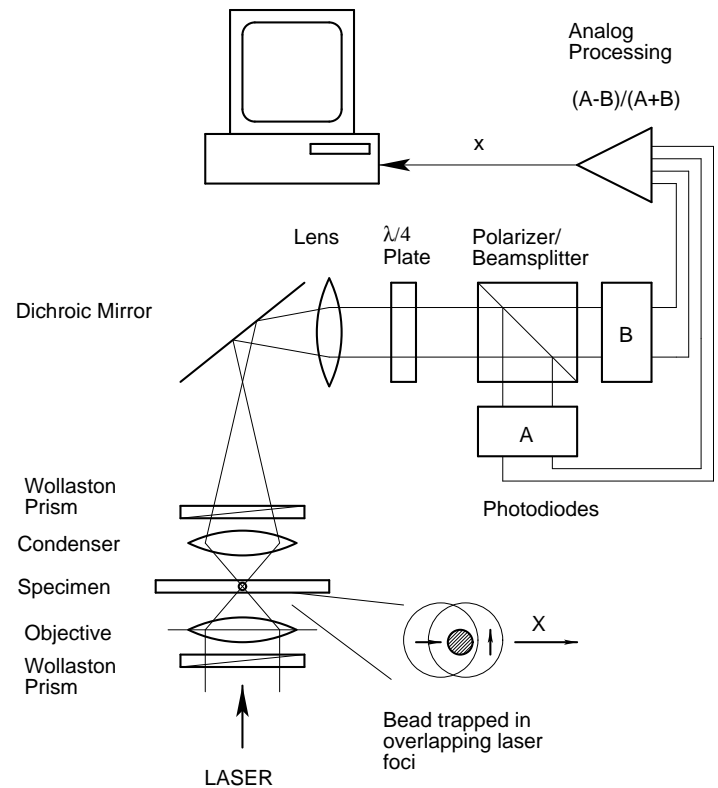


Figure 3: Schematic diagram of the interferometric displacement detection system.

terface (MIO 16X, National Instruments) and data acquisition software written in Labview (National Instruments).

Although this is not done here, the focused laser beam can act, at high enough laser power, as an optical trap, exerting forces on the particle in the focus<sup>44,45</sup>. Here, we want to measure unperturbed thermal fluctuations, and thus need to minimize the trapping force. For that purpose, a 1.5 mm diameter pinhole was inserted at a position conjugate to the back focal plane of the objective, broadening the laser focus and increasing the detector range. The laser power was typically 0.6 mW in the specimen, low enough to make optical forces negligible.

Before recording fluctuations of an individual bead, it was centered in the detector range using a piezo-actuated translation stage. For all experiments reported here, the data acquisition rates were 50 or 60 kHz (anti-alias filtered at 25 kHz). Time series data were recorded for at least 17.5 seconds ( $2^{20}$  data points) to obtain power spectra ranging from 0.1 Hz to 25 kHz. Each spectrum was evaluated by Fast Fourier Transform (FFT) after applying a Welch window. Power spectra were smoothed by averaging within bins of geometrically increasing width (with factor 1.1).

The linear range of the detector is about 200 nm for

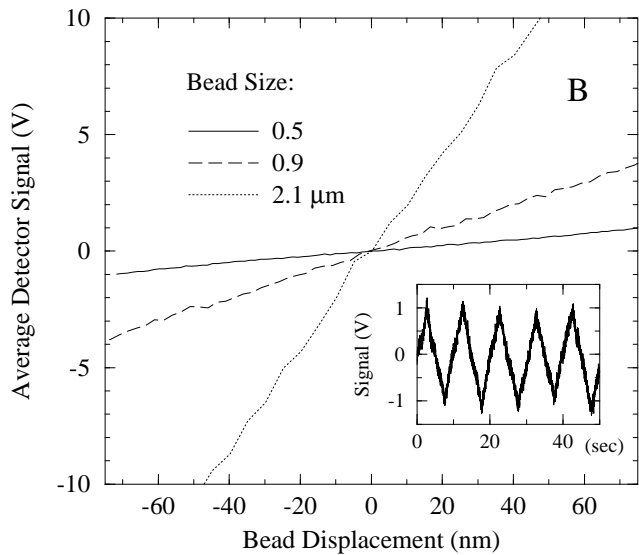
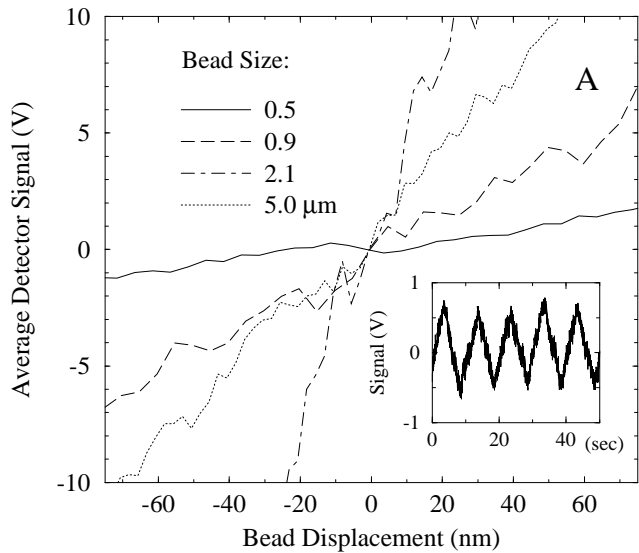


Figure 4: Detector sensitivity for displacement of silica beads of various diameters embedded (A) in an actin solution (2 mg/ml F-actin) and (B) in a 2.5% PAAm gel, determined by driving a piezo-actuated stage with a triangular signal at a frequency of 0.1 Hz. Response curves are averages over several periods, sampled at 100 Hz (inset), smoothed (by a Savitsky-Golay filter) and shifted vertically to pass through the origin. For a uniform scale some curves include a gain factor. Inset: Direct signal time series for a 0.5  $\mu\text{m}$  bead.

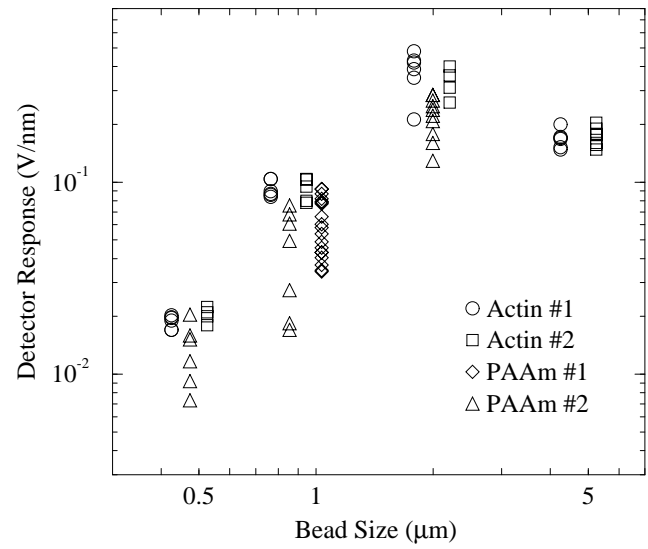


Figure 5: Bead-size dependence, and scatter, of detector response factors (see Fig. 4). Four different experiments are compared; two with F-actin and two with PAAm. Data points are horizontally shifted for clarity. Vertical scatter is partly due to bead polydispersity, but PAAm experiments show a distinctly stronger scatter. Bead diameters are 0.5, 0.9, 2.1, and 5.0  $\mu\text{m}$ .

0.5  $\mu\text{m}$  beads and increases with bead size. Each observed bead was immediately calibrated following the recording of thermal motion, by moving the sample on the piezo-actuated stage with a triangular signal wave form, producing constant velocity displacements (between 150 nm and 1  $\mu\text{m}$  peak-to-peak) at a frequency of 0.1 Hz. The driving voltage was digitally synthesized to correct for the non-linearity and hysteresis of the piezo actuators. Driver voltage (not shown) and detector response (Fig. 4 inset) were recorded for about 40 seconds and analyzed by plotting detector response versus bead displacement. Slopes were estimated by linear regression from an averaged response-displacement curve for each individual bead (Fig. 4A and B). The result is a sensitivity factor which is used to convert detector signals into actual displacements.

While centering the bead in the detector range, we found that the sensitivity does not vary strongly in the perpendicular direction (Y), out to Y-offsets comparable to the linear range. The sensitivity also did not vary significantly with axial position in a range for which the bead appeared focused in the video image ( $\sim 0.6 \mu\text{m}$ ). Detector sensitivities as a function of bead diameter are plotted in Fig. 5. They increase roughly with the third power of bead radius as long as the bead is smaller

than the laser focus, since the scattering amplitude is expected to scale with the volume of the scatterer. For larger beads (in the limit of geometrical optics), the sensitivity decreases roughly as  $R^{-1}$ , the only remaining length scale. In other words, the same relative displacement  $\Delta x/R$  should give the same signal  $\Delta V$ , independent of bead size:  $\Delta V \propto \Delta x/R$ .

Investigating the origin of scatter in the detector sensitivity, we found that variations in beam alignment dominated bead polydispersity for the actin experiments. Bead polydispersity was checked directly with transmission electron microscopy (TEM; data not shown) and found to be about 10%, with a non-normal distribution. The images showed both larger beads, which appear to have formed by merging nuclei, and very small beads that may be contamination. The scatter in the displacement-response slopes was about  $\pm 10\%$  (coefficient of variation) for actin. When no correlation was evident between calibration factors and the amplitudes of the PSD at around 100 Hz (which should scale with bead radius  $R$ ) we averaged the factor over all beads observed in a sample.

For PAAm the scatter in sensitivities for a given bead size appeared significantly larger ( $\pm 30\text{-}60\%$  coefficient of variation), and response factors were indeed correlated with the PSD, indicating that at least part of the scatter was caused by bead size polydispersity. In these cases, spectra were calibrated by the factors determined for individual beads, which decreased the variance in the spectra between beads in the same sample. Since the response factor scales roughly with the third power of bead diameter for the smaller beads (see Fig. 5), a 10% coefficient of variance can explain a 30-40% scatter in the spectra. The polymer network itself and possible surface adsorption is not expected to influence apparent bead size and thus sensitivity substantially. Furthermore, the index of refraction changes little with polymer volume fraction in PAAm (measured to be about a 1.2% increase in relative index of refraction at 10% polymer w/v). Finally, surface chemistry that could produce a dense layer of polymer directly on the bead surface is not expected to produce more than a monolayer, and is thus limited to a thickness on the order of tens of Å.

## Results

### Actin solutions

Fluctuation time series were recorded for silica beads of 0.5, 0.9, 2.1, and 5.0  $\mu\text{m}$  diameter, embedded in actin gels of 1 and 2 mg/ml concentrations. The fluctuation signal is well above the noise, as shown by comparison

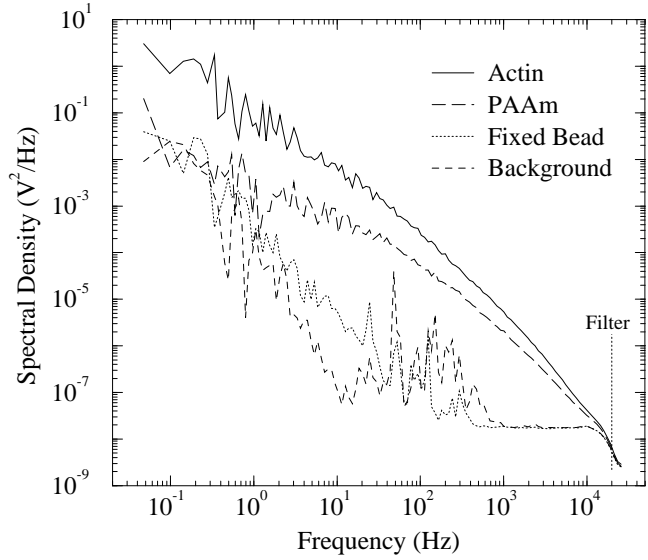
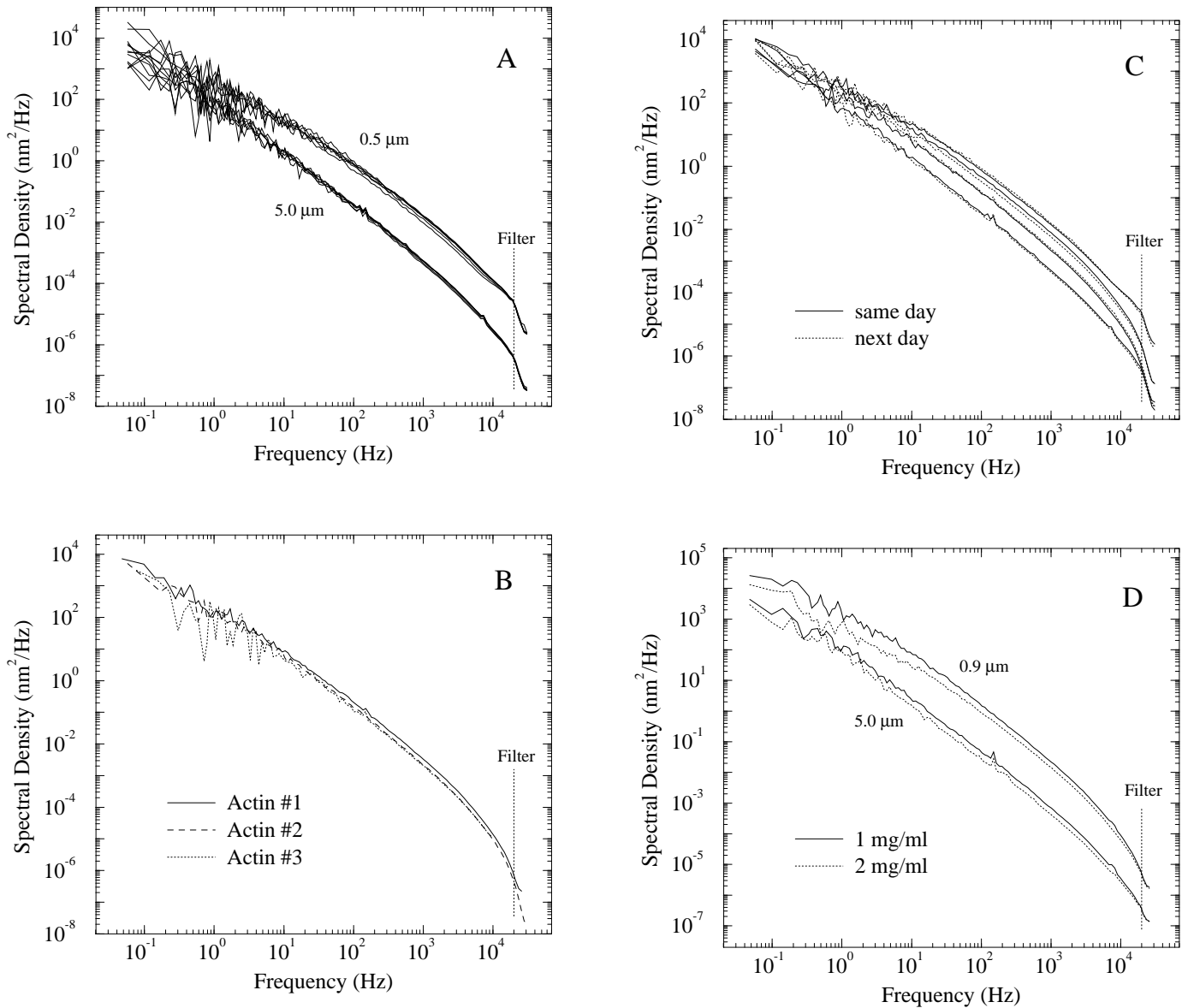


Figure 6: PSDs (power spectral densities) of background noise compared to signal for F-actin and PAAm. Voltage signals were sampled at 50 kHz and spectra were smoothed by averaging in equal log bins. An anti-aliasing filter attenuates the signal strongly above about 20 kHz. The lower two curves show the PSD of the interferometer signal for water without bead, and with a 0.5  $\mu\text{m}$  bead fixed on a glass surface. The F-actin spectrum (0.5  $\mu\text{m}$  bead in 2 mg/ml actin) is everywhere about two orders of magnitude above the noise, whereas the PAAm spectrum (0.5  $\mu\text{m}$  beads in 2% PAAm) is dominated by noise below about 1 Hz.

to spectra of a bead immobilized on a surface, and of the water background without bead (Fig. 6). These controls display the effects of low-frequency instrumental noise due to thermal drifts in the microscope and the laser beam path, acoustic vibrations, and beam-pointing fluctuations. At high frequencies, noise depends on laser intensity since detection shot noise and preamplifier noise are dominant there. We emphasize that the amplitude of this noise is small, and remains about two orders of magnitude below the signal. Note that all spectra are (analog) anti-alias filtered at 25 kHz, causing the “tails” at about 20 kHz.

The power spectra of bead fluctuations in actin solutions were reproducible in shape and amplitude between different beads in the same sample (Fig. 7A), as well as between samples (Fig. 7B). Observed coefficients of variance (of the PSD at 100 Hz in Fig. 7A) within a sample ( $N=6$ ) were 22% (0.5  $\mu\text{m}$ ), 24% (0.9  $\mu\text{m}$ ), 8.7% (2.1  $\mu\text{m}$ ) and 15% (5.0  $\mu\text{m}$  bead diameter). Fig. 7B shows two spectra from samples in different experiments but from



the same protein preparation, and one made with actin from a different laboratory (sample provided by Paul Janmey). We find that beads in different samples do not scatter more than different beads within one sample.

Slow changes have been reported to occur in actin solutions over many hours after polymerization, possibly due to the depletion of ATP in the buffer, or to the annealing of filaments. To address such effects, we remeasured samples the day following their preparation, without seeing significant differences in the spectra (Fig. 7C). Observed beads were typically located at heights between 10 and 50  $\mu$ m above the sample chamber surface. Variations in the spectra were not correlated with distance from the boundaries (data not shown).

Power spectral densities (PSDs) of thermal motions of

Figure 7: (A) Reproducibility within individual samples of F-actin (2 mg/ml). Six beads each with diameter 0.5 and 5.0  $\mu$ m. Height above the sample cell surface was between 10 and 50  $\mu$ m. (B) Reproducibility between experiments and different protein preparations. Spectra from two experiments using the same actin preparation at a concentration of 2 mg/ml (#1: 1.8  $\mu$ m, #2: 2.1  $\mu$ m silica beads) and using actin from a different laboratory (P. Janmey) (#3: 1.8  $\mu$ m silica beads). (C) Aging of F-actin samples. Spectra from four samples (0.5, 0.9, 2.1, 5.0  $\mu$ m beads, top to bottom, with six beads averaged per sample) measured within hours of polymerization and remeasured the following day. (D) Comparison of 1 and 2 mg/ml F-actin solutions. Spectra from two samples with 0.9  $\mu$ m beads and two samples with 5.0  $\mu$ m beads. Six beads are averaged in each plotted PSD.

0.9 and 5.0  $\mu\text{m}$  silica beads in actin solutions at different concentrations are shown in Fig. 7D. The shape of 1 and 2 mg/ml spectra is similar and the PSD amplitude of the less concentrated sample is smaller, as expected.

A phase transition to a nematic phase has been reported for actin at concentrations of about 2 mg/ml<sup>40,46</sup>. However, we see no qualitative difference in the appearance or in the behavior of our actin gels at 1 and 2 mg/ml. There were no signs of inhomogeneities under polarization microscopy. Furthermore, we do not see any greatly increased scatter in our measured values of  $G^*$ , which would be expected in a highly anisotropic medium, given our uniaxial detection technique.

Fig. 8A shows averaged and smoothed spectra obtained from 2 mg/ml actin solutions with beads ranging from 0.5 to 5.0  $\mu\text{m}$  in diameter. The variance in the smoothed spectra (values at 100 Hz) as a function of bead diameter is plotted in the inset. Part of the scatter presumably reflects local inhomogeneities in the networks. Smaller beads, which probe more locally, should show more scatter. For 0.5  $\mu\text{m}$  beads, however, some variation is also due to drift out of the linear range of the detector, and to bead polydispersity, as discussed in Materials and Experimental Methods. Detector sensitivity depends on bead size, as we have shown in Fig. 5. The high frequency noise level follows this dependence, with the smallest (0.5  $\mu\text{m}$ ) and largest (5.0  $\mu\text{m}$ ) beads showing the largest relative noise levels.

The largest beads are about a factor of 10 to 20 larger than the average mesh size (0.25  $\mu\text{m}$  for actin at 2 mg/ml<sup>47</sup>) and a continuum elastic model should apply. Approximate power law behavior, with a slope of about  $-1.75$ , is evident over about three decades in frequency for the 5  $\mu\text{m}$  beads, as indicated in Fig. 8. All spectra show a slight downturn at about 3 kHz, an effect which we cannot yet explain. At the high frequency end, the data have not reached the noise bottom evident in the spectrum of a bead fixed to the substrate surface (Fig. 6).

Eq. (5) predicts that spectra should scale with the bead radius  $R$  for high frequencies. This is roughly observed as shown in Fig. 8B, but a systematic deviation from  $R$ -scaling is evident. Small beads show power spectral densities of higher amplitude than expected. We believe that the increased fluctuations are not due to diffusion through the network or constraint release due to filament reptation; in video recordings of up to two hours we did not observe any long-range diffusive motion. Furthermore, we can exclude that the beads themselves bind to F-actin (with potential bunching of filaments as a result), because we observed practically unimpeded diffusion of silica beads (0.2  $\mu\text{m}$ ) with diameters below the

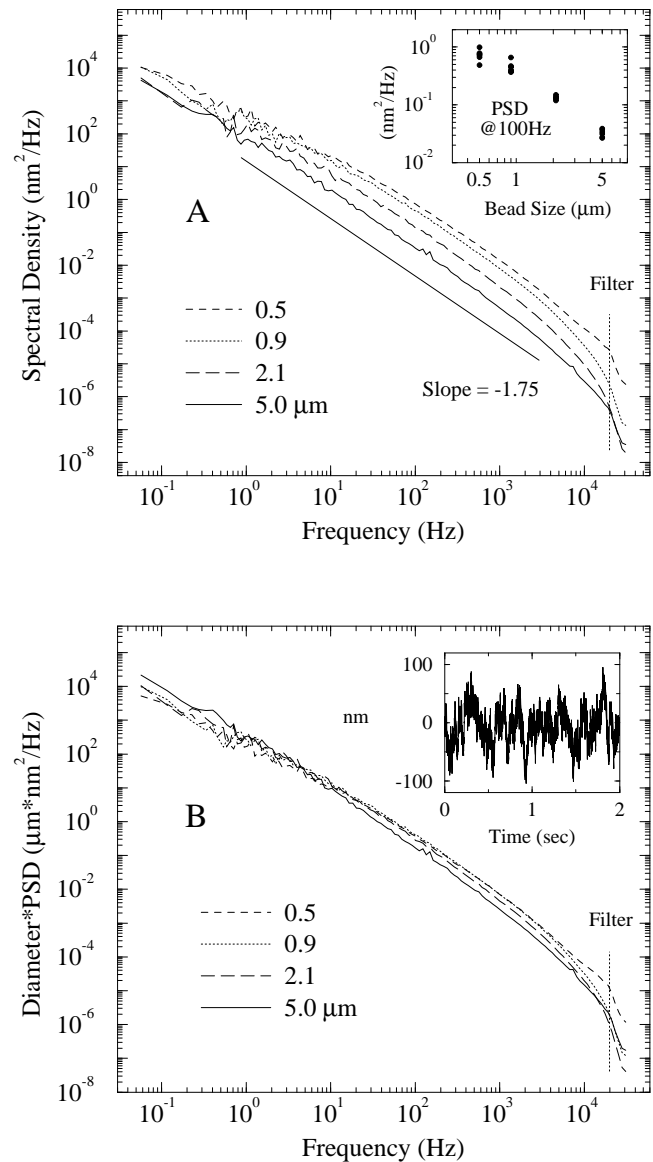


Figure 8: (A) Bead-size dependence of PSDs in 2 mg/ml F-actin solutions using a 60 kHz sampling rate. Spectra were calibrated with response factors found as in Fig. 4. PSDs from beads between 0.5 and 5.0  $\mu\text{m}$  diameter are shown. For each bead size PSDs from six different beads in one sample were averaged. The line indicates a power-law slope of  $-1.75$ . Inset: PSD amplitudes at 100 Hz of individual smoothed spectra that make up the averages. (B) Averaged PSDs from (A) multiplied by their respective bead diameters. Inset: direct time series data for 0.9  $\mu\text{m}$  bead.

mesh size.

We instead attribute the lack of scaling to the steric exclusion of filaments near the bead. This model is elaborated quantitatively in a separate publication<sup>34</sup> but given qualitatively in the following. A large bead of radius  $R$  will affect the distribution of filaments to an exclusion depth  $\ell \sim \ell_p$ , where  $\ell_p$  is the filament persistence length. Since the Stokes flow field around a large bead extends beyond the exclusion depth to a distance on the order of  $R$ , large beads will mainly see the unperturbed network according to Eq. (5). Small beads ( $R \ll \ell_p$ ) will exclude filaments to a depth of the order of  $R$ , and thus see an effective compliance larger than that described by Eq. (5). Once in this limit, the compliance should again scale as  $R^{-1}$ . This is consistent with our observations: the spectra for the smaller beads (0.5 and 0.9  $\mu\text{m}$ ) do indeed superimpose after scaling (Fig. 8B).

At low frequencies the slopes of the spectra decrease, and the PSDs converge for all beads (Fig. 8A). The onset of the slope change, however, *does* depend on bead size. Therefore, for the actin samples it can *not* be the onset of the elastic plateau as is the case for the PAAm data shown below. Instead, we interpret the change in slope as the transition, predicted by Eq. (4), from a regime of pure shear fluctuations to long-wavelength draining modes, for which the spectra should become bead-size independent<sup>34</sup>. Such a transition is not seen in PAAm because the smaller mesh size inhibits draining. The estimate for the crossover frequency for our F-actin solutions—on the order of 10 Hz—is also consistent with the data.

Fig. 9A-D show the storage and loss shear moduli  $G'(\omega)$  and  $G''(\omega)$  obtained for various bead sizes in 2 mg/ml actin solutions by evaluating the Kramers-Kronig integral, Eq. (7). The continuum model should apply to the largest beads (Fig. 9D) which are about 20 times larger than the mesh size. There, scaling is observed directly in both  $G'$  and  $G''$  in the range from about 5 to 100 Hz. Pure scaling corresponds theoretically (via Eqs. (5) and (7)) to a complex modulus  $G^*(\omega) \propto (i\omega)^z$ , so that their ratio is  $G''/G' = \tan \pi z/2^4$ . This ratio, averaged between 10 and 100 Hz for the largest beads (Fig. 9D), allows a precise estimate of  $z = 0.75 \pm 0.02$ .

Eqs. (5) and (6) imply scaling of the power spectrum, via Eq. (11), as  $\langle x_\omega^2 \rangle \propto \omega^{-1.75}$ , consistent with the apparent slope in (Fig. 8A). The scaling exponent  $z$  of about 3/4 in the macroscopic behavior is distinct from the predictions of Rouse-like scaling with exponent 1/2 observed for flexible polymers (see PAAm below). We are unaware of any existing model that predicts  $z = 3/4$  for the scaling of the complex, macroscopic shear mod-

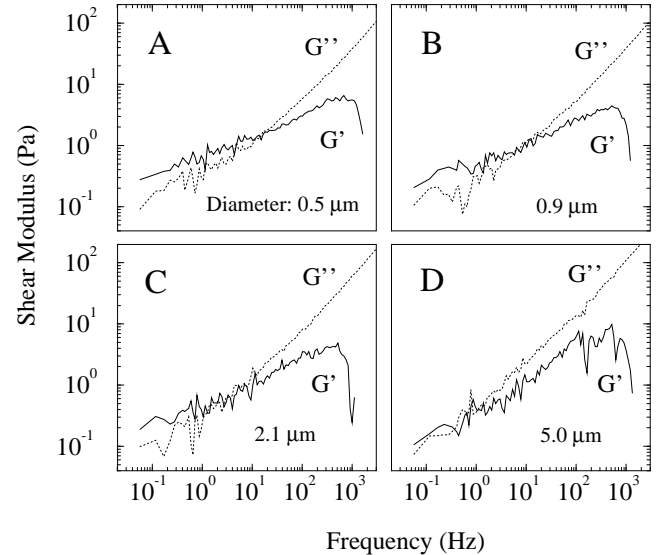


Figure 9: (A-D) Real and imaginary parts of the complex shear modulus of 2 mg/ml actin solutions, obtained from the spectra in Fig. 8 via the Kramers-Kronig relation (Eq. (7)) for bead diameters 0.5, 0.9, 2.1 and 5.0  $\mu\text{m}$ . Power law scaling of the complex shear modulus emerges for the largest beads (D). At low frequencies, an elastic plateau is not yet apparent.

ulus.

We also note that no plateau is (yet) visible in  $G'(\omega)$ . To compare with the literature, we quote values at the lowest frequencies we observed.  $G'$  at 0.1 Hz was  $0.11 \pm 0.03$  Pa for 1 mg/ml and  $0.17 \pm 0.07$  Pa for 2 mg/ml (actin). Ruddies *et al.*<sup>15</sup> measured a value of  $G' \approx 0.3$  Pa near the observed onset of the plateau in 0.3 mg/ml actin.

For smaller beads, the apparent  $G'(\omega)$  and  $G''(\omega)$ , calculated under the assumptions of a single fluid behavior, show deviations from macroscopic shear elastic behavior (Fig. 9ABC), and a pure scaling regime is not reached in the data. This confirms that the assumption of an incompressible network is not valid over the whole frequency-range of the spectra for the smaller beads.

## Polyacrylamide gels

Polyacrylamide gels, even at volume fractions close to the gelation threshold, are so rigid that we approach the limits of our technique. Given the noise floor illustrated in Fig. 6, our technique is limited at present to static shear moduli of up to a few hundred Pascal. A volume fraction of 2% (with relative crosslinker concentration of 3%) was the lowest concentration that resulted in reproducibly solidified gels. Fig. 10 shows PSDs of 0.9  $\mu\text{m}$

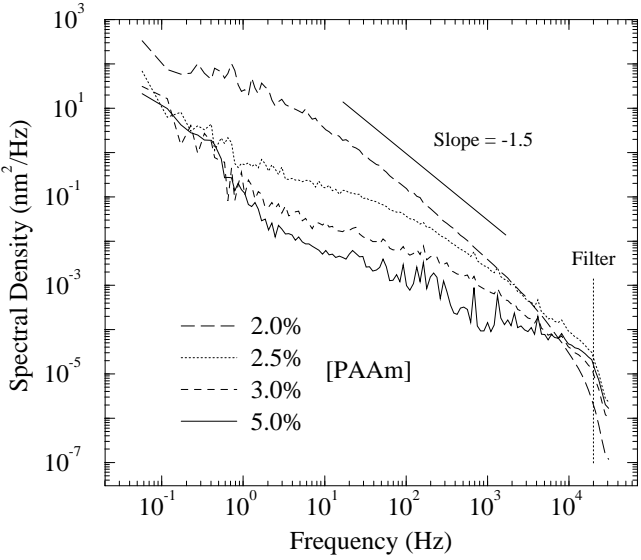


Figure 10: Concentration dependence of PSDs for  $0.9\text{ }\mu\text{m}$  beads in PAAm gels. The PSD from the 5% gel is substantially affected by instrumental noise. The line indicates a power law slope of  $-1.5$ . The onset of the elastic plateau is visible as a concentration-dependent change in slope at low frequency.

beads embedded in 2, 2.5, 3, and 5% (volume fraction) PAAm gels, linearly averaged over several beads respectively, and log-binned as described in Materials and Experimental Methods. Absence of long-range diffusion of the beads confirms that all gels were crosslinked into solids. Since the mesh size in the PAAm gels (about 5 nm in the 2% gels<sup>48</sup>) is in all cases much smaller than the bead size, a continuum elastic model is expected to apply throughout.

PSDs for beads in the softest gels (2%) show a power law slope of about  $-1.5$  near 100 Hz, which is distinctly less steep than in F-actin. We again observe the slight but unexpected downturn in the spectra above about 3 kHz. The flattening of the spectra below a few Hertz reflects the elastic plateau (compare Fig. 11A). This plateau extends higher for stiffer gels. For concentrations above 2.5%, instrumental noise begins to dominate the low-frequency part of the spectra (and approaches the fixed-bead spectrum, see Fig. 6). Raising the PAAm concentration higher above the gelation threshold leads to dramatically increased gel rigidity, making the observation of fluctuation signals above the noise difficult. After calibrating the spectra with the sensitivity factors determined for each bead (see Fig. 5), the scatter in the spectra typically remained large, unlike for actin. The inset in Fig. 13 shows PSDs at 1 Hz for different bead

sizes in 2.5% gels, indicating this large scatter.

The 2 and 2.5% gels are not much above the gelation threshold and the gel rigidity there changes very rapidly with concentration. Therefore, the observed scatter is presumably partly due to local gel inhomogeneities. Bead polydispersity, as discussed in Materials and Experimental Methods, is a further contribution. As for actin, we find no correlation with distance from the substrate surface. The calculated frequency-dependent storage moduli for the data in Fig. 10 are shown in Fig. 11A. The transformation Eq. (7) has largely eliminated unphysical low-frequency noise in these spectra, allowing the plateau modulus  $G'(\omega \rightarrow 0)$  to be easily estimated. For 2, 2.5, 3, and 5% gels the plateau values of  $G'$  are approximately 2.0, 24, 100, and 280 Pa.

The effective scaling of  $G'$  with concentration is 1.8 (for concentrations between 3 and 5%), and steeper for lower concentrations. Our 2.5% gels thus lie in a regime of very rapidly increasing stiffness indeed (this is consistent with Ref. 49). For larger plateau moduli the upturn shifts, as expected, to higher frequencies. The pure scaling regime beyond the plateau is not reached for any of the samples, although its existence is suggested by the slope of  $-1.5$  in the PSDs. The corresponding scaling of  $G'(\omega) \propto \omega^{1/2}$  is consistent with the Rouse model<sup>4</sup>.

Fig. 11B shows the results of control experiments performed with conventional cone-and-plate rheology (courtesy of M. Osterfield, J. Shah, P. Janmey). Samples were prepared following the same recipes as for the microrheological experiments. Plateau values agree within a factor of 2-3. The data show qualitatively the same steep dependence on concentration as the microrheological results. Elastic plateaus are clearly visible for 2.5 and 3% gels whereas for the 2% gels instrumental limits are reached, as seen from the large scatter of the data.

Fig. 12A shows averaged spectra for different bead sizes (between 0.5 and  $2.1\text{ }\mu\text{m}$ ) in 2.5% PAAm gels; in Fig. 12B these power spectra are multiplied by the respective bead diameters. The  $R^{-1}$ -dependence in Eq. (5) predicts that the rescaled curves have the same shape and magnitude. This is approximately true for the central frequencies in the spectra, but the high rigidity of the PAAm gels causes non-displacement noise to be significant both at high frequencies (electronic detection noise) and low frequencies (thermal drifts, laser beam-pointing and mode instabilities, etc.). The parts of the spectra that are dominated by noise show no scaling. Due to the bead-size dependence of the detector sensitivity, the low-frequency noise extends higher for smaller beads.

The storage moduli  $G'(\omega)$  for three different bead sizes 2.5% gels are shown in Fig. 13(inset). In contrast to

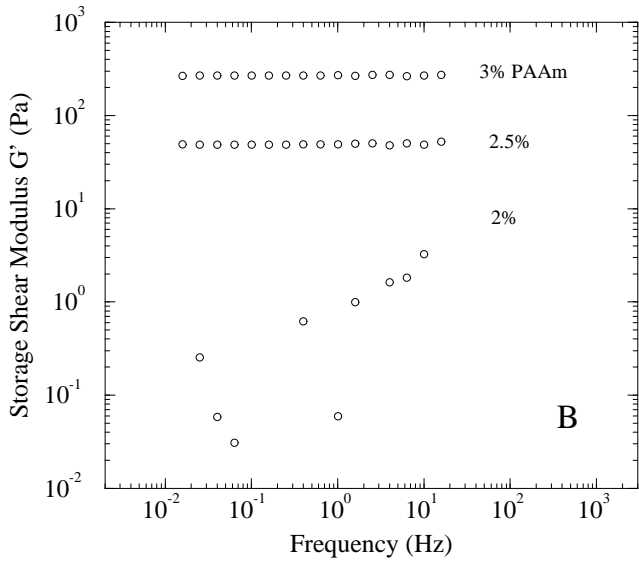
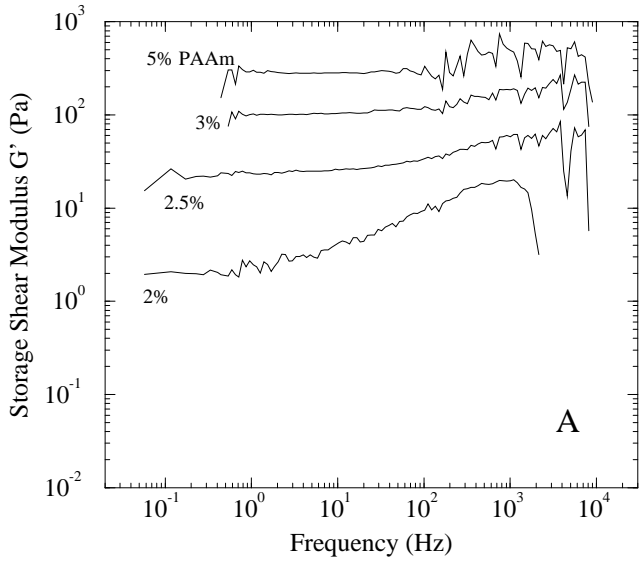


Figure 11: (A) Concentration dependence of the storage modulus in PAAm gels, obtained from the spectra in Fig. 10. Moduli were calculated for individual beads and linearly averaged. Elastic plateaus are clearly visible and their extent is found to increase with gel concentration. The vertical range is chosen to match (B). (B) Control experiments with a cone-and-plate rheometer (Rheometrics RFS II Fluids Spectrometer) with PAAm gels prepared in a manner identical to the samples in (A). Forced oscillatory measurements were made at 1% strain and at 25°C (data courtesy of M. Osterfield, J. Shah, and P. Janmey).

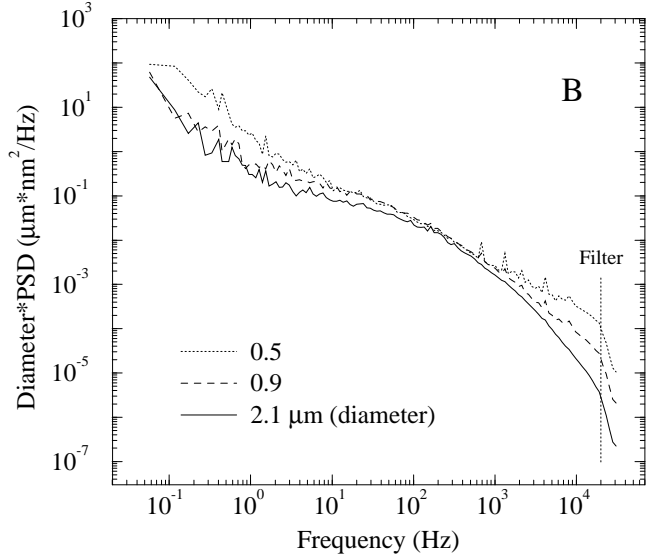
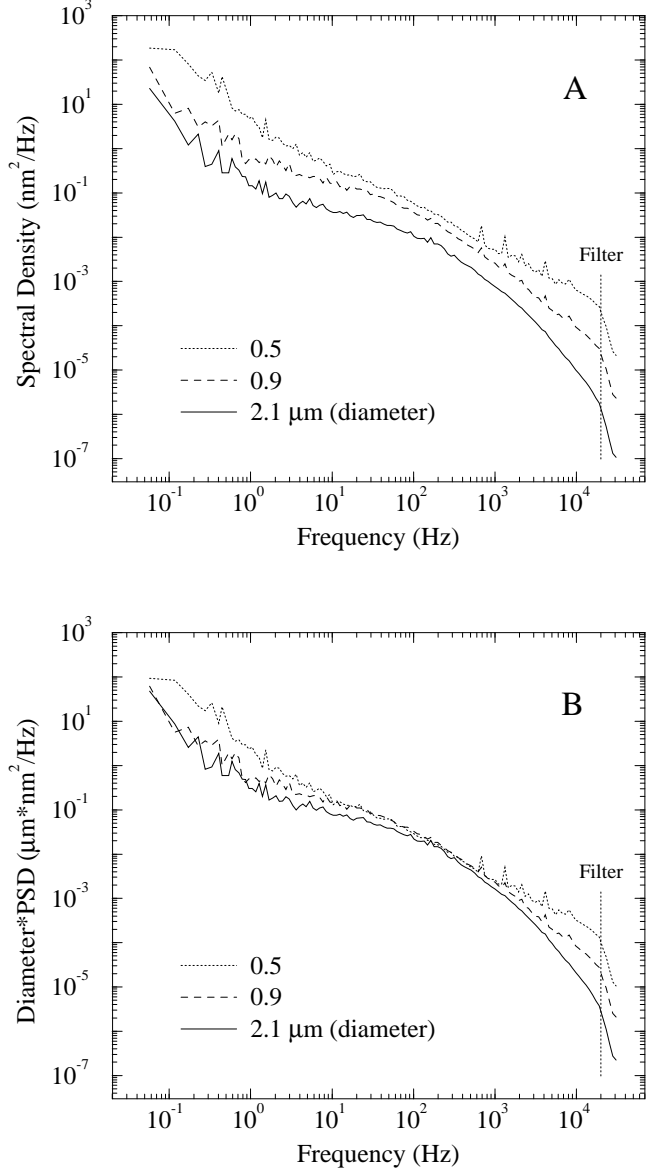


Figure 12: (A) Bead-size dependence of PSDs, for beads in PAAm gels of 2.5% concentration. Spectra for 0.5, 0.9 and 2.1  $\mu\text{m}$  bead diameters are averaged over 6, 7 and 10 beads respectively. (B) Averaged PSDs from (A) multiplied by their respective bead diameters.

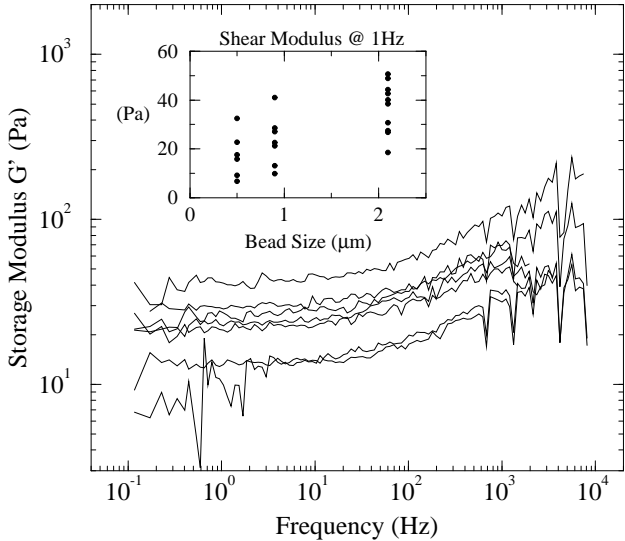


Figure 13: Variation in the storage modulus of 2.5% PAAm gels, for seven different  $0.9\text{ }\mu\text{m}$  beads. The substantial scatter may be partly due to bead polydispersity. Inset: Values of  $G'$  at 1 Hz for multiple beads of three sizes.

what was found for actin, the elastic plateau is clearly visible for all samples, and agrees for different bead sizes in the same concentration to within about a factor of 2. The elastic plateau extends to about the same frequency for all bead sizes. This is in contrast to the low-frequency slope changes in actin, which we interpret as finite-mesh-size effects, supported by a consistent bead-size dependence. With mesh sizes as small as in PAAm, draining effects should not play a role, down to the lowest frequencies we measure. However, the trend in the data is to show apparently smaller moduli for smaller beads. We attribute this artifact to a remaining sensitivity to noise in the integration procedure used to calculate  $G'$ . The detector sensitivity decreases dramatically for smaller beads, thus including more noise in the integral, leading to the underestimate of  $G'$ . The plateau moduli estimated by the value of  $G'$  at 1 Hz (Fig. 13) are 36 Pa (2.1  $\mu\text{m}$ ), 24 Pa (0.9  $\mu\text{m}$ ), and 17 Pa (0.5  $\mu\text{m}$  bead diameter).

## Discussion

We have introduced the direct use of the Kramers-Kronig dispersion integral Eq. (7) to obtain storage and loss moduli from power spectra of thermal motions. Other methods have been used to obtain shear moduli from the thermal mean-square particle displacement as a function of time: Mason and Weitz give

an approximate method based on real-valued Laplace transforms<sup>28</sup>; Mason and Wirtz describe a somewhat different approximation<sup>29,50</sup>. A limitation of the former method is that a specific functional form was postulated, fitted to a numerical Laplace transform of particle displacement data, and then analytically continued to the Fourier domain. Possible systematic errors in such a scheme are not known. Such transformation methods have previously been shown to be sensitive to noise and to behavior at the frequency extremes<sup>51</sup>. In contrast with Ref. 28, we have applied the transforms described in Eqs. (5) and (8) directly to our measured spectra. Both of these transform methods are sensitive to the frequency extremes, but we believe that the direct transformations we have employed are better controlled.

In order to demonstrate the dependence of our Kramers-Kronig transformation on the limits of the integration interval, we show in Fig. 14 the transformation of a model power spectrum that decreases as a power of frequency, above a corner frequency that we arbitrarily place at 0.1 Hz. We choose the power law to be  $\omega^{-1.75}$ , similar to the power law observed in our fluctuation power spectra for actin solutions. This model spectrum corresponds, theoretically, to a complex modulus  $G^*$  that increases as  $G^* \propto \omega^{0.75}$  above the corner frequency, and a plateau in the storage modulus  $G'$  below the corner frequency. We show in Fig. 14 the results of a transformation carried out with various values of the upper and lower cutoffs. The effect of cutoffs is minimal in the central portion of the transforms.

The shear elastic storage and loss moduli ( $G'$  and  $G''$ ) we found for actin solutions are consistent with other experiments<sup>26,27</sup> in the frequency regime where they can be compared. Other reported techniques have been limited in frequency to a maximum of about 10 Hz. Discrepancies persist in the literature,<sup>16</sup> and values up to 300 Pa have been measured for F-actin at a concentration of 2 mg/ml. We did not observe changes in viscoelastic behavior in F-actin over periods of at least 24 hours after polymerization. This suggests that the local properties of the solutions probed by the micron-sized beads are not affected by slow network changes. On the other hand, macroscopic techniques which have observed such changes may not have probed the linear response regime.

Actin microrheology by others<sup>26</sup> could be interpreted as consistent with  $\omega^{3/4}$  scaling, although the authors there suggest  $\omega^{1/2}$  scaling; the frequencies observed were close to the onset of the plateau. Macrorheological work<sup>15,19</sup> has also reported  $G^* \sim \omega^{1/2}$ . Here too, the frequencies studied may have been in the transition between plateau and scaling regime. New results from mul-

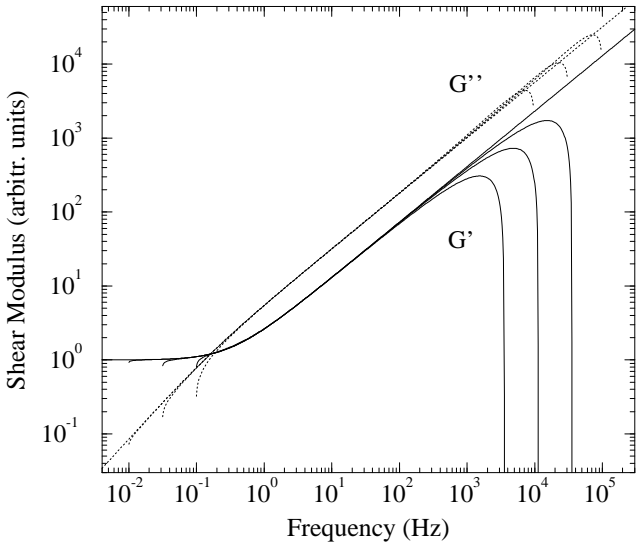


Figure 14: Frequency-cutoff dependence of the Kramers-Kronig transformation on a model spectrum. The model PSD (not shown) decreases as  $\omega^{-1.75}$  above a corner frequency at 0.1 Hz. The same Kramers-Kronig transformation and complex inversion are performed as on the actual data in Fig. 9, resulting in the storage and loss moduli  $G'$  and  $G''$ . The lower cutoffs are at  $10^{-2}$ ,  $10^{-1.5}$ , and  $10^{-1}$  Hz, and the upper cutoffs are at  $10^4$ ,  $10^{4.5}$ , and  $10^5$  Hz. For comparison, the curves without any cutoff are also included. Deviations from the correct curve extend up by about a factor of 2 from the lower cutoff and down by about a factor of 10 from the upper cutoff. Our actual data in Fig. 9 have an input frequency range similar to the curve cut off at  $10^{-1.5}$  Hz and  $10^{4.5}$  Hz.

multiple light scattering experiments (D. Weitz, personal communication) are consistent with a scaling exponent close to  $3/4$  at even higher frequencies than we are able to measure. This scaling behavior in semiflexible actin solutions may be a universal property of this type of network, but is so far unexplained. In particular, there is no reason to expect Rouse or Zimm scaling in these systems<sup>4</sup>. Bead dynamics in actin networks consistent with the power spectra we observe have also been reported in the limit of very dilute gels (specifically, for  $R \simeq \xi$ )<sup>25</sup>; the authors suggest a model based on single filament dynamics. We believe that at the (higher) concentrations we used, for which the mesh size is substantially smaller than bead diameters, our continuum elastic approach is correct.

For solutions of semiflexible polymers, where effective entanglement lengths may be much larger than the mesh size,<sup>52,53</sup> crosslinking is expected to have a very strong effect on the gel rigidity. In cells, the actin cortex is extensively crosslinked while the average filament length is short. Therefore, a rigidity relevant for cell biology has to be measured with a crosslinked actin gel, potentially lessening the discrepancies between reported measurements.

In both F-actin solutions and PAAm gels, one might expect to be able to resolve local inhomogeneities in viscoelastic parameters with increasingly smaller beads. We did see considerable scatter in the fluctuation power spectra, but this spread did not increase for smaller beads, as one might have expected. Therefore the inhomogeneities in the systems we studied may be smaller than effects of bead polydispersity and other instrumental errors. More extensive statistical characterization of the probe particles and improvement of the instrument will reduce the noise, as well as increase the available frequency range. These improvements will allow closer examination of sample inhomogeneities.

Our PAAm gels were very close to the gelation threshold and therefore expected to be inhomogeneous. For gels of 2, 2.5, 3, and 5% we indeed find a very steep increase in  $G'$  (Fig. 15). This qualitative behavior and the absolute values are consistent with our control experiments with cone-and-plate rheology and the data match literature values in the 3-5% range<sup>49</sup>. Macroscopic methods tend to get inaccurate for low shear moduli on the order of 1 Pa, whereas our microscopic method underestimates shear moduli above 100 Pa (stiff gels) due to noise in the bead position detection.

In PAAm, the scaling of  $G^*(\omega) \propto \omega^{1/2}$  is reflected by an apparent power law slope of  $-1.5$  in the spectra, consistent with the Rouse model<sup>4</sup>.

A current limitation of our method, so far unex-

plained, is a steepening of the power spectrum that we consistently observe above a few kHz. We believe this is an artifact, because it occurs even for beads in pure water. We have ruled out electronic filtering as a cause. This effect translates, in the Kramers-Kronig transformation of Eq. (7), to a sharp plunge in the calculated storage modulus at high frequency, which is of course unphysical. Again, this illustrates the subtle nature of the frequency sensitivity of the Kramers-Kronig and related transformations. Although the downturn in our spectra occurs in the vicinity of 10 kHz, its effects are apparent in  $G'(\omega)$  approximately one decade below this.

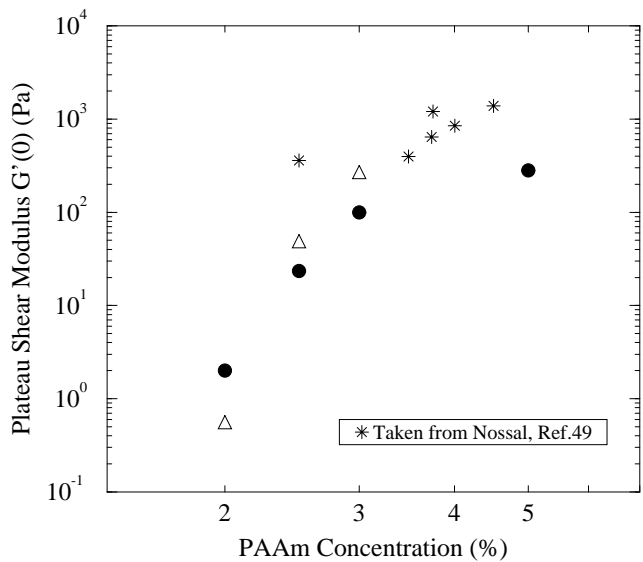


Figure 15: Storage shear modulus of PAAm as a function of gel concentration. Solid circles: Microrheology results, values estimated from the plateaus in Fig. 11A. Open triangles: Cone-and-plate rheology (data courtesy of M. Osterfield, J. Shah, and P. Janmey), values estimated from the plateaus in Fig. 11B. Stars: Values taken from Ref. [49], obtained from dynamic light scattering, with a crosslinker fraction of 0.026, similar to our 3% preparation.

## Conclusions

We have used thermal fluctuations of micron-sized probes to measure local properties of polymer solutions, by a passive and thus non-invasive method, particularly appropriate for labile biopolymers. Laser interferometry provides dynamic measurements of probe displacements with high resolution and up to frequencies not previously explored for F-actin solutions. With probes that are large compared to the mesh size of the network, macroscopic properties such as the complex shear modulus  $G^*(\omega)$  can be estimated from the power spectrum of fluctuations by using dispersion relations from linear response theory. This analysis is made possible by our large detection bandwidth. By sampling micron-sized volumes we can in principle map out spatial inhomogeneities in soft polymer systems.

Probes of sizes on the order of the mesh can be used to observe deviations from macroscopic behavior, for example the transition to microscopic filament dynamics. Observing this breakdown of continuum elasticity may be of fundamental importance for understanding the origins of elasticity in polymer systems, and has been the subject of very recent theoretical attention<sup>54–56</sup>. Furthermore, we have shown that our technique (like other microrheological methods using probe particles in polymer solutions) is predicted to be limited at low frequencies—at least in measuring *macroscopic* shear moduli. This is because of expected draining dynamics of network-plus-polymer, which is not apparent in macroscopic rheometric methods. On the other hand, inertial effects of both probe and solvent, typically a problem in sensitive macroscopic instruments,<sup>1</sup> occur only at MHz frequencies in microscopic experiments.

On the micron length scale, a bead in a network should behave somewhat like an organelle suspended in the cytoskeleton of a biological cell, and we expect that the method will be transferable to measurements in living cells, where biological processes are expected to strongly

modify viscoelastic parameters. Our technique is currently limited by broadband (mainly acoustic) noise to rather soft materials, up to shear moduli of a few hundred Pascal. This limitation will be extended by technical improvements. Meanwhile, much remains to be done in developing a theoretical understanding of the semiflexible polymer systems.

## Acknowledgements

This work was supported in part by the Whitaker Foundation, the National Science Foundation (Grant Nos. BIR 95-12699 and DMR 92-57544), and by the donors of the Petroleum Research Fund, administered by the ACS. We thank M. Osterfield, J. Shah, and P. Janmey for providing macroscopic rheological data for controls, and P. Janmey for a control batch of actin. We acknowledge generous technical support from the Rowland Institute for Science, particularly by W. Hill. We thank G. Tank and J. Langmore for help with the electron microscopy, and P. Olmsted, P. Janmey, J. Käs, A.C. Maggs, and D. Weitz for helpful discussions. FCM also wishes to thank the Aspen Center for Physics.

## References

- [1] Ferry, J. D. *Viscoelastic Properties of Polymers*; Wiley: New York, 1980.
- [2] Bird, R. B. *Dynamics of Polymeric Liquids*; Wiley: New York, 1987.
- [3] Larson, R. G. *Constitutive Equations for Polymer Melts and Solutions*; Butterworths: Boston, 1988.
- [4] Doi, M.; Edwards, S. F. *The Theory of Polymer Dynamics*; Clarendon Press: Oxford, 1988.
- [5] Graessley, W. W. *The Entanglement Concept in Polymer Rheology*; Springer-Verlag: Berlin, 1974.
- [6] Alberts, B.; Bray, D.; Lewis, J.; Raff, M.; Roberts, K.; Watson, J. D. *Molecular Biology of the Cell*; Garland Publishing, Inc.: New York, 1994.
- [7] Stossel, T. P. *Sci Am* **1994**, *271*, 54-55, 58-63.
- [8] Gittes, F.; Mickey, B.; Nettleton, J.; Howard, J. *J. Cell Biol.* **1993**, *120*, 923-934.
- [9] Ott, A.; Magnasco, M.; Simon, A.; Libchaber, A. *Phys. Rev. E* **1993**, *48*, R1642-1645.
- [10] Pollard, T. D.; Goldberg, I.; Schwarz, W. H. *J. Biol. Chem.* **1992**, *267*, 20339-20345.
- [11] Wachsstock, D. H.; Schwartz, W. H.; Pollard, T. D. *Biophys. J.* **1993**, *65*, 205-214.
- [12] Sato, M.; Leimbach, G.; Schwarz, W. H.; Pollard, T. D. *J. Biol. Chem.* **1985**, *260*, 8585-8592.
- [13] Zaner, K. S.; Hartwig, J. H. *J. Biol. Chem.* **1988**, *263*, 4532- 4536.
- [14] Newman, J.; Zaner, K. S.; Schick, K. L.; Gershman, L. C.; Selden, L. A.; Kinosian, H. J.; Travis, J. L.; Estes, J. E. *Biophys. J.* **1993**, *64*, 1559- 1566.
- [15] Ruddies, R.; Goldmann, W. H.; Isenberg, G.; Sackmann, E. *Europ. Biophys. J.* **1993**, *22*, 309-321.
- [16] Janmey, P. A.; Hvidt, S.; Käs, J.; Lerche, D.; Maggs, A.; Sackmann, E.; Schliwa, M.; Stossel, T. P. *J. Biol. Chem.* **1994**, *269*, 32503-32513.
- [17] Janmey, P. A.; Hvidt, S.; Peetermans, J.; Lamb, J.; Ferry, J. D.; Stossel, T. P. *Biochem* **1988**, *27*, 8218-8227.
- [18] Janmey, P. A. *J Biochem Biophys Methods* **1991**, *22*, 41-53.
- [19] Müller, O.; Gaub, H. E.; Bärmann, M.; Sackmann, E. *Macromolecules* **1991**, *24*, 3111-3120.
- [20] MacKintosh, F. C.; Käs, J.; Janmey, P. A. *Phys. Rev. Lett.* **1995**, *75*, 4425-4428.
- [21] Freundlich, H.; Seifriz, W. *Z. Phys. Chem.* **1922**, *104*, 233.
- [22] Crick, F.; Hughes, A. *Exp. Cell Res.* **1950**, *1*, 37-80.
- [23] Zaner, K. S.; Valberg, P. A. *J. Cell Biol.* **1989**, *109*, 2233- 2243.
- [24] Amblard, F.; Yurke, B.; Pargellis, A.; Leibler, S. *Rev. Sci. Instr.* **1996**, *67*, 818-827.
- [25] Amblard, F.; Maggs, A. C.; Yurke, B.; Pargellis, A. N.; Leibler, S. *Phys. Rev. Lett.* **1996**, *77*, 4470-4473.
- [26] Ziemann, F.; Rädler, J.; Sackmann, E. *Biophys. J.* **1994**, *66*, 2210-2216.
- [27] Schmidt, F. G.; Ziemann, F.; Sackmann, E. *Eur. Biophys. J.* **1996**, *24*, 348-353.
- [28] Mason, T. G.; Weitz, D. A. *Phys. Rev. Lett.* **1995**, *74*, 1250.
- [29] Mason, T. G.; Dhople, A.; Wirtz, D. In *Mat. Res. Soc. Symp. Proc.* R. H. Austin, T. C. Halsey and D. Wirtz (Ed.), *Boston, 1996*; MRS.
- [30] Stokich, T. M.; Radtke, D. R.; White, C. C.; Schrag, J. L. *J. Rheology* **1994**, *38*, 1195-1210.
- [31] The theoretical aspects of the microrheological technique described here will be treated further in a separate publication<sup>34</sup>.
- [32] Landau, L. D.; Lifshitz, E. M. *Theory of Elasticity*; 3rd ed., Pergamon Press: Oxford, 1986.

[33] Gittes, F.; Schnurr, B.; Olmsted, P. D.; MacKintosh, F. C.; Schmidt, C. F. **1997**, *preprint*.

[34] Gittes, F.; Schnurr, B.; Schmidt, C. F.; MacKintosh, F. C. **1997**, *in preparation*.

[35] Schnurr, B.; Gittes, F.; Olmsted, P. D.; Schmidt, C. F.; MacKintosh, F. C. In *Mat. Res. Soc. Symp. Proc.* R. H. Austin, T. C. Halsey and D. Wirtz (Ed.), *Boston*, 1996.

[36] Milner, S. T. *Phys. Rev. E* **1993**, *48*, 3674-3691.

[37] Brochard, F.; de Gennes, P. G. *Macromolecules* **1977**, *10*, 1157-1161.

[38] Landau, L. D.; Lifshitz, E. M.; Pitaevskii, L. P. *Statistical Physics*; Pergamon Press: Oxford, 1980.

[39] Press, W. H. *Numerical Recipes in C : the Art of Scientific Computing*; Cambridge University Press: Cambridge, New York, 1992.

[40] Käs, J.; Strey, H.; Tang, J. X.; Finger, D.; Ezzell, R.; Sackmann, E.; Janmey, P. A. *Biophys. J.* **1996**, *70*, 609-625.

[41] Pardee, J. D.; Spudich, J. A. In *Structural and Contractile Proteins (PartB: The Contractile Apparatus and the Cytoskeleton)*; *Meth. Enzymology*, D.W. Frederiksen and L.W. Cunningham (Ed.); Academic Press, Inc., San Diego 1982; Vol. 85, p 164-181.

[42] Bio-Rad Laboratories *US/EG Bulletin* 1156.

[43] Denk, W.; Webb, W. W. *Appl. Opt.* **1990**, *29*, 2382-2391.

[44] Svoboda, K.; Schmidt, C. F.; Schnapp, B. J.; Block, S. M. *Nature* **1993**, *365*, 721-727.

[45] Svoboda, K.; Block, S. M. *Annu. Rev. Biophys. Biomol. Struct.* **1994**, *23*, 247-285.

[46] Furukawa, R.; Kundra, R.; Fechheimer, M. *Biochem* **1993**, *32*, 12346-12352.

[47] Schmidt, C. F.; Bärmann, M.; Isenberg, G.; Sackmann, E. *Macromolecules* **1989**, *22*, 3638-3649.

[48] Fawcett, J. S.; Morris, C. J. O. R. *Separ. Sci.* **1966**, *1*, 9-26.

[49] Nossal, R. *Rubber Chemistry and Technology* **1988**, *61*, 255-268.

[50] Mason, T. G.; Ganesan, K.; Wirtz, D.; Kuo, S. C. **1997**, *preprint*.

[51] Chu, B. *Laser Light Scattering - Basic Principles and Practice*; Academic Press: San Diego, 1991.

[52] Semenov, A. N. *Chem. Soc. Faraday Trans. 2* **1986**, *82*, 317-329.

[53] Maggs, A. C. **1997**, *preprint*.

[54] Rubinstein, M.; Ajdari, A.; Bastide, J.; Leibler, L. *Makromol. Chem.- Macromol. Symp.* **1992**, *62*, 61-73.

[55] Barriere, B. *J. Phys.* **1995**, *5*, 389-398.

[56] Elleuch, K.; Lequeux, F. **1997**, *preprint*.